The role of optimality in characterizing CO_2 seepage from geological carbon sequestration sites

Andrea Cortis, Curtis M. Oldenburg, and Sally M. Benson

Earth Sciences Division 90-1116

Lawrence Berkeley National Laboratory,

Berkeley, CA 94720, USA.

August 7, 2007

Revised: February 29, 2008

Abstract

Storage of large amounts of carbon dioxide (CO_2) in deep geological formations for greenhouse-gas mitigation is gaining momentum and moving from its conceptual and testing stages towards widespread application. In this work we explore various optimization strategies for characterizing surface leakage (seepage) using near-surface measurement approaches such as accumulation chambers and eddy covariance towers. Seepage characterization objectives and limitations need to be defined carefully from the outset especially in light of large natural background variations that can mask seepage. The cost and sensitivity of seepage detection are related to four critical length scales pertaining to the size of the: (1) region that needs to be monitored; (2) footprint of the measurement approach, and (3) main seepage zone; and (4) region in which concentrations or fluxes are influenced by seepage. Seepage characterization objectives may include one or all of the tasks of detecting, locating, and quantifying seepage. Each of these tasks has its own optimal strategy. Detecting and locating seepage in a region in which there is no expected or preferred location for seepage nor existing evidence for seepage requires monitoring on a fixed grid, e.g., using eddy covariance towers. The fixed-grid approaches needed to detect seepage are expected to require large numbers of eddy covariance towers for large-scale geologic CO_2 storage. Once seepage has been detected and roughly located, seepage zones and features can be optimally pinpointed through a dynamic search strategy, e.g., employing accumulation chambers and/or soil-gas sampling. Quantification of seepage rates can be done through measurements on a localized fixed grid once the seepage is pinpointed. Background measurements are essential for seepage detection in natural ecosystems. Artificial neural networks are considered as regression models useful for distinguishing natural system behavior from anomalous behavior suggestive of CO_2 seepage without need for detailed understanding of natural system processes. Because of the local extrema in CO_2 fluxes and concentrations in

natural systems, simple steepest-descent algorithms are not effective and evolutionary computation algorithms are proposed as a paradigm for dynamic monitoring networks to pinpoint CO_2 seepage areas.

1. Introduction

1. Global climate change motivation

The current trend of carbon dioxide (CO_2) emissions in the atmosphere has been associated with an increase in the average land and ocean temperatures, and represents an increasing danger for the stability of Earth's climate (e.g., Hansen, 2004). To address this concern, various Carbon Capture and Storage (CCS) technologies have been proposed to capture CO_2 at point sources such as power plants, cement plants, and oil refineries to avoid emissions into the atmosphere. Among these, capture with sequestration in deep geological formations (such as depleted oil and gas reservoirs, and brine formations) appears to be promising (IPCC, 2005). In this work, we focus on the optimization of near-surface monitoring and measurement strategies for characterizing seepage from geologic storage sites. This study presupposes the importance of seepage characterization in general without specifying which particular objectives, e.g., safety, environmental impact, storage verification, etc., are motivating any particular effort (see e.g., Benson, 2006).

2. The monitoring and measurement challenge

Leakage to the atmosphere of a significant fraction of injected CO_2 would constitute a failure of a geological CO_2 storage project from a greenhouse gas mitigation perspective (Hepple and Benson, 2005). In the terminology of Oldenburg and Unger (2003, 2004), leakage is the escape of (some fraction of) CO_2 from the intended subsurface storage reservoir to other regions of the subsurface, while seepage is the escape of the CO_2 into the atmosphere. Seepage may include high-flux discharges through wells and faults or low-flux, diffuse seepage through the land surface. The fundamental quantities we consider monitoring and measuring to characterize

seepage are flux or concentration where both can be of CO_2 alone or of a co-injected tracer, or some isotopic fraction indicative of the injected CO_2. In order to ensure safety and effectiveness of geologic CCS, storage sites, monitoring needs to be carried out at some level of detail so that seepage can be detected and roughly located. If monitoring detects CO_2 seepage, then strategies for additional measurements to pinpoint and quantify the seepage event(s) can be deployed. In a world of limited resources, the surface monitoring and measurement challenge is to ensure the effectiveness and safety of CCS through field measurements with minimal economic and near-surface environmental impact.

3. The seepage detection problem

In order to achieve an effective mitigation of CO_2 greenhouse-gas effects by sequestering CO_2, billions of tons of CO_2 need to be safely stored in the next 50 years (Pacala and Socolow, 2004). The typical annual CO_2 emission from a 1 GWatt coal-fired power plant (sufficient to satisfy the electricity needs of approximately one million people) is approximately 10^{10} kg/yr. Assuming that the CO_2 from this single power plant is stored in a supercritical state with a density of 700 kg/m^3, this corresponds to a volume equal to 1.4 x 10^7 m^3. Assuming a thickness of the geologic storage region equal to 10 m, porosity equal to 10%, and pore occupancy equal to 10%, the radius of the corresponding cylindrical volume is about 2 km after one year, and after 30 years of injection will be in the order of tens of km. Because of the large areas of the subsurface that may be in contact with the injected CO_2, there is concern for leakage along faults in the cap rock or through abandoned wells. There is also some concern among the public that geologic CCS is potentially dangerous due to the potential for CO_2 seepage (Shackley, et al., 2007).

From these considerations, monitoring will be an essential component of CCS projects. Hepple and Benson (2004) effectively described the scope of such a monitoring program as follows:

"An effective monitoring program should focus first on detecting whether or not emissions are occurring. Once emissions, or the possibility for emissions are detected, a more intense effort can be made to precisely locate and quantify them. Designing a monitoring program in the first instance to quantify emission rates would be unnecessarily costly and, if emissions were to occur, unlikely to provide as reliable data as a tailored program would be."

In this work, we adopt the above philosophy, although we distinguish *monitoring* as the activity involved in detecting and locating seepage areas from *directed measurements* that are made to pinpoint and quantify seepage once it is detected. We emphasize that in order to be effective at detecting seepage, a monitoring program must be affordable enough to carry out and therefore requires optimization. Further, we elucidate how, from a design point of view, the *detection* problem needs to be kept distinct from the *optimization of the detection* problem. Note that this paper is focused on monitoring and measurements for detecting, locating, and quantifying seepage at the land surface and does not address characterizing leakage out of the primary storage reservoir. Different approaches, primarily pressure monitoring and geophysical techniques (e.g., Myer et al., 2002) are needed to detect leakage from the storage reservoir and are not the subject of this paper.

2. Static and dynamic monitoring networks

1. Assumptions and strategies

There are two possible approaches to the analysis of seepage. The first approach is to assume that seepage is present. In this case, we need to detect, locate, pinpoint, and quantify the seepage, and we need to find optimal ways to carry out these tasks. The second point of view is to assume that seepage is not necessarily present. In this case, the tasks are to identify the minimum target for detection, and use the best strategy to optimize detection. The first approach could lead to

exorbitant costs in the case that monitoring is carried out in the attempt to detect a seepage signal that is non-existent. The second approach is the one we adopt and is the most applicable to geologic CCS for which seepage is going to be very unlikely due to careful site selection and operations. It is also essential to differentiate between the (*i*) *potential for*, (*ii*) the *possibility of*, and (*iii*) *actual* seepage. The difference is not purely academic as it implies widely different deployment strategies as described below. Note that we assume that seepage has reached a pseudo-steady-state in both the static and dynamic network discussions below.

2. Static networks

In case (*i*) (above), the *potential for* seepage, a priori information about the site (e.g., presence of a fault in the caprock, unsealed wellbores, seismicity of the area) will be available and suggestive of potential seepage. In this case we need to design a *static* monitoring network (such as a grid of eddy covariance (EC) towers) for the area of potential leakage. Based on the cost of the corresponding monitoring network, a decision would have to be made about whether the cost of the network allows adoption of that particular site in the first place.

Static monitoring networks require optimization only in a loose sense. In fact, the sensitivity required of the monitoring network will determine the spacing of the measurements and their frequency. Finite spacing and measurement frequency give rise to systematic error in a static network applied to a dynamic and heterogeneous system. A static monitoring network is defined by either one of two criteria: (*1*) a detection limit (e.g., maximum allowed flux or integrated discharge) imposed upon the design of the network; or (*2*) a maximum cost per unit area imposed upon the design of the network. These two interrelated bounds on the optimization of the grid measurement density may or may not result in creating an effective monitoring network.

3. Dynamic networks

In case (*ii*), the *possibility of* seepage, we assume that we are operating already at some injection site for which we have evidential support of anomalous CO_2 flux or concentration relative to a reliable baseline data set (e.g., CO_2 fluxes or concentrations on a fixed grid at the surface, or pressure measurements at the injection borehole do not conform to theoretical predictions). It is important to note that the anomaly could be natural in origin and unrelated to the CO_2 storage site. Regardless of the cause of the anomaly, we need to put in place a *dynamic* approach to pinpoint its location. We define a *dynamic* (as opposed to a *static*) network as a strategy of directed measurements aimed at precisely locating (pinpointing) anomalies. For this reason, establishing a *dynamic* network is a good strategy only if we have a priori information about the existence of anomalies. Dynamic networks adapt future spatial sampling and frequency of measurement according to the history of measurements. An example of a dynamic network might be the tracking of a CO_2 soil-gas concentration or flux gradient until a maximum concentration is found. Dynamic networks are more efficient at precisely locating CO_2 seepage because they can eliminate the systematic errors that are typical of static networks.

Finally, in the case of *actual* seepage (case *iii*), we need to distinguish the following two sub-cases: (*a*) seepage has been pinpointed and quantified, but the fluxes or concentrations are not a cause of concern for safety or effectiveness; *(b)* seepage has been pinpointed and assessed, and its levels are unacceptable in terms of safety, environmental impact, or effectiveness. In (*a*), the two main stakeholders involved are the carbon credit regulator and the operator. In (*b*), though arguably the most dramatic in its practical consequences, such seepage is the easiest case for monitoring. The consequences of a CO_2 geyser, of a dying forest, or of animal losses and human casualties are easily assessed without the need of a monitoring network, much less an optimized

one. The practical consequences of such an occurrence will not be any different than for any other industrial accident, i.e., shutdown of operations, access restrictions, and deployment of mitigation and remediation actions. In this case, optimization efforts shift from monitoring to mitigation efforts.

3. Measurements and length scales

1. Instruments

For the sake of this study on characterizing seepage in the near-surface environment, we consider deployment of standard instruments for concentration and flux measurement. In particular, we presume that soil-gas samples can be taken from shallow soil and analyzed using infrared absorption techniques to determine CO_2 concentration in the soil gas. In addition, LiDAR (Light Detection and Ranging) can be used above ground to measure CO_2 concentration in the air. For flux measurements, we assume that accumulation chamber (AC) approaches are used to measure local CO_2 flux from the ground surface, and eddy covariance (EC) can be used for measuring surface fluxes over larger areas. Because each instrument has its own strengths and uses, monitoring and measurement strategies are tightly linked to the choice of instrument. Reviews of measurement and monitoring instrumentation relevant to geologic CCS have been presented elsewhere (Oldenburg et al., 2003; IPCC, 2005; Shuler and Tang, 2005).

2. Spatial Support

When addressing CO_2 monitoring measurements, it is essential to consider the spatial support of the measurement. For instance, AC measurement may only be representative of an area of tens of square centimeters (Chiodini et al., 1998); a LiDAR measurement represents an integral measure along a line (Radziemski, 1987; Schlessinger, 1995; Shuler and Tang, 2005); an EC tower yields an average over some footprint area (Anderson and Farrar, 2001; Baldocchi and Wilson, 2001; Massman and

Lee, 2002; Foken and Wichura, 1996; Gouldin and Crill, 1997). Each of these measurement spatial support scales has characteristic advantages and disadvantages. While a point measurement precisely addresses conditions at some given spatial point, a large number of point measurements may be necessary to obtain an adequate representation of a given area. On the other hand, EC gives an integral value over a surface area, albeit of varying size and location depending on atmospheric conditions. In other words, if the seepage area has a small footprint dimension, EC can be used to detect an anomaly without being necessarily able to precisely locate it. Point measurements can be more precise in locating and quantifying seepage, but heterogeneity complicates interpretation and spatial integration. The same problem described for flux for EC holds also for concentration measured using LiDAR which provides an integral over a line measurement.

For all of the above reasons, it is useful to define typical ratios of spatial scales to elucidate effectiveness and sensitivity of different monitoring and measurement approaches. Monitoring systems must be characterized by at least four length scales as follows:

- L_x, the typical linear dimension of the maximum extent of the region of investigation;
- L_m, the typical linear dimension of the footprint of the monitoring approach;
- L_s, the linear dimension of the main area of seepage;
- L_i, the typical linear dimension of the area influenced by seepage.

Figure 1 illustrates these four length scales with shading to represent deviations from baseline fluxes or concentrations. Two different L_m scales are shown to represent, e.g., the difference between EC and AC approaches. The lightest gray indicates noise-level deviations from the baseline and represents the region where the baseline is evaluated. The intermediate shade

indicates an area with significant deviations from the baseline that are increasing towards the darkest area, a region where there are large deviations due to seepage. L_i is an important length scale for point and linear measurements as it defines the region over which a gradient search is possible.

If we assume that the dynamic search is started inside the area of influence (of length scale L_i) and we follow some effective search direction, we are certain that we will detect the seepage anomaly represented by the dark region of length scale L_s. On the other hand, if the starting point for the dynamic search is very far away from the area of influence, there is no possibility of evaluating a gradient and therefore no basis for a preferred search direction to pinpoint the seepage anomaly of length scale L_s. Furthermore, if $L_s \sim L_i$, there is very little chance that an observer monitoring points far away from the seepage area will eventually reach the anomaly in a simple dynamic search. If the anomaly is detected, seepage can be quantified by increasing the density of measurements in its immediate proximity.

To make these length scale considerations more quantitative, it is useful to assume a simplified conceptual model of the storage reservoir in which the injected CO_2 volume is distributed uniformly in the pore-space and where buoyancy and dissolution effects are neglected. We also assume that the CO_2 background is due to photosynthesis and respiration which typically show significant diurnal and daily variations as functions of solar radiation (in its direct and diffuse components), meteorological conditions (e.g., precipitation, wind speed and direction, humidity, air pressure), soil, and vegetation type. Anthropogenic carbon sources such as those derived from neighboring industrial or transportation activities may also significantly affect background CO_2 levels. Temporal variations in the CO_2 fluxes occurring at a given location can be de-trended by standard signal processing tools such as Fourier or wavelet transforms to discriminate long-term

trends, and cycles and anomalies can be detected by means of a de-noising process (Lewicki et al., 2005).

Figure 2 shows simulations of net CO_2 flux performed with the ISOLSM model (Riley et al., 2002; 2003) for the typical conditions of the Morgan-Monroe State Forest, Indiana, USA (Ehman et al., 2002). The simulations reproduce the very large diurnal variations in the net CO_2 flux that are typically observed in field conditions, and the more regular night-time daily evolution (in red) of respiration. The annual average night-time respiration flux for this forest is thus on the order of j_r = 5 μmol m^{-2} s^{-1}, and this sets a level of sensitivity for any anomalous measurements of CO_2 flux in this area.

We assume now an injection program designed for a 1 GW coal-fired power plant, which corresponds to a mass M injection rate of $CO_2 \sim 10^{10}$ kg/yr. The molar injection rate I is equal to

$$I = \frac{10^{10}}{3.1536\times10^{7}}\frac{kg}{s}\frac{1}{44\times10^{-3}}\frac{mol}{kg} \approx 7.2\times10^{3}\frac{mol}{s} \qquad (1).$$

If we assume that the formation volume occupied by CO_2 is equal to a cylinder of radius r, (regardless of the actual number of wells needed to achieve this injection rate) and volume $V = Ah = \pi r^2 h$, the radius as a function of injection rate is given by

$$r = \sqrt{\frac{M\,N}{n\,po\,\rho\,\pi h}} \qquad (2)$$

where N is the number of years of injection. Assuming a formation thickness h = 100 m, porosity n = 0.1, pore occupancy po = 0.1, and a density for the supercritical CO_2 equal to ρ = 700 kg m^{-3},

we obtain a radius of $r \sim 2$ km after 1 year and 11 km after 25 years. It has been suggested that annual losses due to leakage must be less than 0.1% (10^{-3}/yr for the CCS process to be effective if CCS is deployed at a large scale (Hepple and Benson, 2005). This maximum annual release fraction (R) is not the amount of CO_2 that will leak, but rather an upper limit on leakage below which storage is still effective as an approach for climate change mitigation. In order to be detectable, the allowed seepage flux (j_a) should be significantly larger than the average respiration flux (j_r) by an amount given by an amplification factor (λ) where $\lambda = (j_a + j_r)/j_r > 1$. The amplification factor is a measure of the precision with which seepage flux can be distinguished from the background respiration flux. If a very robust and precise method can detect seepage (j_a) at levels on the order of j_r, then λ would be approximately equal to two. Using the definition of the seepage flux

$$j_a = \frac{R\,I\,N}{A_i} \sim \frac{R\,I\,N}{L_i^{\,2}} \qquad (3)$$

and substituting the definition of λ for j_a in Eq. 3, we obtain an expression for the order of magnitude of L_m needed to detect a seepage flux for a given λ:

$$L_m \sim L_i \sim \sqrt{\frac{R\,I\,N}{\lambda\, j_r - j_r}} \qquad (4).$$

Equation 4 states that the EC measurement footprint required to detect the seepage flux is a function of the annual seepage rate, the number of years of injection, amplification factor, and background respiration flux. Note that in this analysis seepage is not required to start contemporaneously with injection. Assuming that $R = 10^{-3}$ yr^{-1}, $I = 7.2 \times 10^3$ mol/s, $N = 25$ yrs, $\lambda = 10$, and $j_r = 5$ μmoles m^{-2} s^{-1}, we obtain $L_m \sim 2$ km. The value of L_m would reduce to 632 m for

a value of $R = 10^{-4}$. From these simple arguments, we can deduce that an EC network with a fixed measurement sensitivity needs to have a spacing smaller or equal to the minimum L_m. Assuming that the CO_2 plume spreads uniformly around the injection well, the number of EC towers (n_{tower}) needed to detect seepage around the well with amplification λ is given by the function

$$n_{tower} = ceiling\left(\left(\frac{r}{L_m}\right)^2\right) \qquad (5)$$

Note that because both r and L_m are proportional to $t^{1/2}$ (Eqs. 2 and 4), n_{tower} is invariant with time. At early times, the towers would be smaller and clustered more tightly than at later times. The number of EC towers for the cases presented above are 29 and 284 for the $R = 10^{-3}$ and 10^{-4} cases, respectively.

Results for L_m at $t = 25$ yr and the corresponding number of EC towers needed are shown in Table 1 for different combinations of the allowable leakage rate and amplification factor with a background respiration flux (j_r) of 5 μmol m^{-2} s^{-1}, porosity of 0.1, pore occupancy of 0.1, reservoir thickness of 100 m, and CO_2 injection rate of 10^{10} kg/yr. Table 2 shows similar results for $j_r = 20$ μmol m^{-2} s^{-1}. As shown in Tables 1 and 2, the number of EC stations becomes very large if it is necessary to detect very small seepage rates at large amplification factors (λ) above background fluxes. Note that the number of EC towers in Tables 1 and 2 are based solely on L_m without regard for practical limitations on EC tower height which put limits on measurement footprint. With novel monitoring approaches as discussed below, seepage at small values of amplification factor may be detectable thereby reducing costs by reducing the number of monitoring stations. The detection limit for EC measurements in biologically active areas may be

as low as 2.7 μmol CO_2 m^{-2} s^{-1} (10 μmol C m^{-2} s^{-1}) above background respiration CO_2 exchanges (Miles et al., 2005; Hagen et al., 2006). Finally, the numbers derived in this analysis should be considered valid only in an order-of-magnitude sense and subject to change depending on local site-specific properties and processes.

4. Mechanistic vs artificial neural network models

1. Introduction

The length-scale analysis presented above is based on some grossly simplifying assumptions. In reality, the shape of the CO_2 plume depends on a number of hydrogeological, geomechanical, topographical, geochemical, and atmospheric properties that have not been taken into consideration when deriving estimates of number of stations needed for the static monitoring network. Constraints on geomechanics, for instance, put limits on the maximum size of a disruptive leak as the maximum injection rate can be bounded by the formation fracturing limit. Hydrogeological properties such as formation permeability, soil diffusivity, and water saturation play a key role in leakage plume evolution, and hence on the final shape and size of the seepage footprint. Vadose zone thickness influences soil water distribution, and hence the distribution of the CO_2 fluxes and concentrations through capillary effects, local distribution of soil and air temperature, solar radiation, and wind exposure. Additionally, topography plays a fundamental role in the distribution of the CO_2 released into the near-surface atmosphere by channeling the denser-than-air CO_2 in valleys, or by wind-induced dispersion in flat areas (Oldenburg and Unger, 2004). If we take into account the variability in CO_2 fluxes that will arise in natural systems and correlate it to easily measured system properties (e.g., topography), we can detect anomalies that may be due to seepage without having to rely on a large amplification factor. By using advanced monitoring approaches as discussed in this section, the number of stations (e.g.,

EC towers) in a fixed grid can be reduced.

2. Mechanistic models

To investigate a more realistic case of seepage characterization that includes a realistic topography and geology, we selected a hypothetical injection site in which we performed numerical simulations of CO_2 seepage. A false-color satellite photo image of the virtual site is shown in Figure 3. This domain (Figure 3) would have been identified through EC monitoring at a larger scale (L_x) as a subregion in which an anomaly was detected in the course of seepage characterization. A 3D numerical simulation of the virtual site was carried out with TOUGH2 (Pruess et al., 1999) using a research module applicable for CO_2-air-water mixtures (Oldenburg and Unger, 2003; 2004) to calculate water saturation assuming a water table with depth ranging from 15-35 m and uniform rainfall infiltration of 100 cm/yr. Uniform porous medium properties were assigned to emphasize the effects of topographic variability. This simulation was carried out to provide a challenging CO_2 seepage detection problem rather than to elucidate hydrogeologic or CO_2 transport processes, and therefore we omit details of the calculation. A small flux of CO_2 (2.3 μmoles m^{-2} s^{-1} (10^{-7} kg m^{-2} s^{-1})) was imposed uniformly at the top of the water table to model background CO_2 flux, whereas in a smaller region ($L_s \sim 200$ m) we imposed a 20-times higher flux intended to simulate the effect of localized CO_2 seepage such as might occur through a leaking well or a point source created by the intersection of two faults. With reference to Figure 1, $L_i \sim L_s$ in this case and the background is noisy making pinpointing of the seepage area very challenging.

The simulation results are shown in Figure 4. As shown in Figure 4b, the soil water saturation correlates strongly with the elevation map (Figure 4a) as expected for a gravity-capillary equilibrium process. Figure 4c shows the CO_2 concentration map at a soil depth of 10 cm which

exhibits a high degree of correlation with the soil-water saturation. At XY coordinates (1000 m, 800 m), the footprint of the seepage anomaly (red colors) that was imposed as a twenty-fold greater CO_2 flux at the water table is observed. We note that CO_2 fluxes (not shown) correlate almost one-to-one with the concentration map. Figure 4d shows the superposition of the CO_2 concentration from the TOUGH2 numerical simulations with a vegetation CO_2 concentration arbitrarily imposed based on the satellite picture of the site shown in Figure 3. The respiration-derived CO_2 concentration effect was arbitrarily defined to be a function of the level of green of the satellite photo. A map of the "hue" green channel ($0 < \varphi < 1$) was extracted from the satellite photo, and the respiration concentration arbitrarily defined as $c_r = 0.3 \exp(-(1- \varphi))$. The reason for adding this particular vegetation component was to include complex spatial features which were independent of the topographic features to which soil moisture, and CO_2 concentration and flux were strongly correlated.

Although we have used simulations of a virtual site, we expect that there will be correlations between soil-water saturation, vegetation type, and CO_2 fluxes and concentrations in actual monitoring applications. Other interesting correlations with other independent variables (e.g., solar radiation, terrain slope and orientation, soil organic carbon content) need to be explored in future studies. Such a mechanistic approach to the CCS problem, however, cannot be easily adapted across different sites. Moreover, each site-specific model will need an expensive characterization effort to understand and model the relevant active physical processes.

In practice, however, it will not be necessary to find the "universal" model for all storage sites. Instead, the concern will be for a particular site under specific conditions. In other words, what is needed is an easily parameterizable model that, given a set of measurements over some

independent variables, will return the background CO_2 flux level. Departures from this model prediction will then be considered flux “anomalies" that can be investigated further to identify seepage events and to pinpoint and quantify.

3. Artificial neural network models

A growing body of knowledge and research is concerned with the issue of finding anomalies in experimental signals, a discipline that goes under the general name of novelty detection. Novelty detection deals with the identification of new or unknown data that a machine-learning system is not aware of during training (Markou and Singh, 2003a; b). Novelty detection treats anomalies in two ways, namely stochastically (e.g., parametric and non-parametric tests) and deterministically (e.g., neural network classifiers). In both instances, automated computer procedures are designed to perform the task of spotting anomalies in regular patterns with combinations of statistical and neural-network-based approaches. Non-linear regression models such as Artificial Neural Networks (ANNs) appear to be very useful for finding anomalous behavior in complex systems such as ecosystems subject to potential CO_2 seepage. In the context of length scales and amplification factors (λ), ANNs can indicate anomalies at lower λ providing the opportunity to decrease the number of monitoring stations in a static network.

Originally devised to function in analogy to the way our brains function, ANNs prove to be very effective in typical tasks that are easy for a human operator, such as voice, visual, and habit recognition but where typical procedural algorithms fail. Typical tasks to which ANNs have been applied are (*i*) regression analysis, (*ii*) pattern recognition and novelty detection, and (*iii*) data filtering, clustering, separation, and compression. What makes ANNs so unique with respect to other computational tools is their capability of learning by example, a typical task where humans perform better than procedural algorithms, especially where the complexity of the data makes the

design of regressive function impractical. In recent years, ANNs have found widespread application in the hydrological literature, especially as regression tools (Govindaraju and Rao, 2000). ANNs have also been used to build a model for water vapor and carbon exchange in a forest ecosystem, which does not require a detailed knowledge of tree physiology (Hagen et al., 2006).

The attraction of using ANNs in a detection problem resides in their ability to generalize results from a given set of observations, i.e., as regressive models, without the need for any detailed mechanistic understanding of the underlying processes. The key idea is therefore to acquire an "integrated background", i.e., a set of CO_2 measurements as a function of other independent variables (e.g., soil-water saturation, elevation, slope, geographic orientation, solar radiation, leaf area index, permeability, etc.) prior to injection (or sufficiently far away from the injection point that they are not affected by seepage) and then to identify anomalies through long-term monitoring that do not correlate with the expected ANN prediction. This definition of anomaly implies (*i*) that the background measurements must be uninfluenced by CO_2 seepage, either by virtue of being made prior to CO_2 injection or at a location away from any potential seepage, (*ii*) the anomaly is relatively constant over time, and (*iii*) that the location and magnitude of the anomaly do not fluctuate significantly with time (steady-state assumptions).

In practice one should implement the ANN procedure steps as follows:

1. Identify a region around the planned injection site that displays sufficient variability in topography and in other independent variables;

2. Measure the integrated background, i.e., the CO_2 levels (flux and concentration) as a function of the desired independent variables either before injection or at a location that is

not influenced by potential CO_2 seepage;

3. Train the ANN on the measurements collected as the integrated background;

4. Validate the ANN by taking additional measurements of the independent variables.

Figure 5 illustrates the distribution of soil-water saturation (black dots) as a function of the elevation for the simulated case study shown in Figure 4. Two simple three-layer feed-forward ANNs with as little as two and three nodes in the hidden layer, respectively, were trained on the elevation inputs and saturation targets. The transfer function was chosen to be equal to $2/(1 + \exp(-2x)) - 1$, in both cases. The ANN regression function can easily be written explicitly with the $s(z)$ (saturation vs elevation) function defined as

$$s(z) \approx \sum_{i=1}^{N} w_{2i} \frac{2}{1+\exp(w_i z - b_i)} + b_{N+1} \qquad (6)$$

where N is the number of nodes. The number of free parameters was four and seven, for the two- and three-layer ANNs, respectively. The results of the ANN modeling are shown in Figure 5. The correlation between the ANN model output (short-dashed and long-dashed lines) and the targets (black dots) was nearly equal to one in both cases, which means that the elevation variable is capable alone of explaining the saturation. Note that a classical multi-linear regression of the form $s \approx \sum_{i=1}^{N} \alpha_i z^i$ cannot perform equally well, because the linear system matrix becomes badly scaled as soon as the number N of free parameters becomes larger than five. Simple ANNs with a small number of nodes can produce excellent data regression. Small values of the regression coefficient, however, indicate the need for the introduction of other explanatory variables.

4. Application of ANNs to anomaly detection

Following step 1 of the procedure sketched above, we select a 100 point grid in the upper left corner of the monitoring domain of Figures 3 and 4 at which locations we virtually sample the soil-water saturation and vegetation "green-level". In Figure 6 we plot with red dots the sampling grid in the NW corner that provides the integrated background model. We then employ a feed-forward ANN with 20 nodes in the hidden layer. From the correlation plot (right panel of Figure 6), we can see that the measurements from the original points (CO_2 concentration) and from the ANN model outputs correlate very well.

If we make an independent line sampling (pink dots along NW-SE trending line), far away both from the original grid and the anomaly, we can see that the model that we have constructed is capable of inferring the CO_2 levels given only the sampling of the soil saturation and vegetation level. This constitutes a validation of the ANN regression as listed in step 4. If we sample in or around the anomaly along a transect (labeled with green dots), we observe that the measured points are now anti-correlated with the ANN model, clearly indicating the existence and location of the anomalous CO_2 concentrations. An anomaly is indicated when the ANN correlations consistently are below a target threshold. Note that this lack of correlation has to be interpreted in some meaningful statistical sense. One measurement point could easily fall out of the best correlation line without necessarily implying the presence of an anomaly. If, however, many neighboring points do not follow the background predictions, the confidence in identifying these points as anomalous increases.

5. Optimization of Seepage Detection

1. Optimal direction problem

In the previous section, we illustrated a procedure aimed at identifying a pseudo-steady seepage

anomaly independent of its magnitude, and how this anomaly corresponds to a minimum in a correlation map between expected and measured values. This correlation map, however, is not known a priori and only partial interpolations about actual measurements can give hints about search directions. The amount of data necessary for establishing a reliable integrated background remains an open question that we plan to address in future studies. The correlation map can be furthermore very noisy and exhibit many local minima that do not correspond to a real anomaly. What is needed is a strategy to indicate the optimal search direction to locate anomalies, a problem we refer to as the optimal direction problem.

Assuming that an anomaly does exist, an assumption that cannot be verified until the detection process has ended, finding the optimal search direction is a challenging task, particularly when the starting point is far from the assumed anomaly. The classical way to search for a minimum on a map is exemplified by the well-known steepest descent algorithm. In this strategy, the next sampling point is identified by finding the steepest path around the prior search point. The steepest gradient search is guaranteed to converge for convex functions to an absolute minimum. If the function, however, is not convex in the search interval, i.e., exhibits multiple extrema, the algorithm will likely not converge unless the initial guess is in the immediate vicinity of the global minimum. In practice, the steepest descent algorithm and its variants perform very well on smooth search landscapes and in the absence of local minima, conditions unlikely to be found in the search for CO_2 in natural ecosystems.

There is, however, an important limitation to the steepest-descent algorithm. When the search landscape is flat and the minimum is localized around a small region with steep access, this class of algorithms fails in finding the minimum. It also fails as soon as the search landscape is very noisy and characterized by many local minima. The choice of the appropriate minimization

algorithm is an important concern when each point is a field measurement and has a significant cost.

Searching along a predefined grid implies that large areas must be evaluated with very small grid intervals, and this is not a particularly good strategy especially for point-type measurements such as those made by accumulation chambers. Our computer simulations (not shown here) suggest that a random search strategy is even more expensive than a predefined grid search with the same number of points. A more sophisticated search strategy is therefore needed.

2. Evolutionary Computation and Swarm Intelligence

Recently, a number of search strategies based on the concept of Evolutionary Computation and Swarm Intelligence have been proposed. Among these strategies, Genetic Algorithms (GA) (Holland, 1992), Particle Swarm Optimization (PSO) (Eberhart and Kennedy, 1995), Ant Colony algorithms (Dorigo and Stützle, 2004), and Differential Evolution (Storn and Price, 1995) algorithms have become very popular because of their effectiveness in finding global minima in noisy search landscapes.

Most Evolutionary Computation algorithms display the following structure:

1. Random generation of an initial population of individuals.
2. Calculation of a fitness value for each individual of the population.
3. Reproduction of the population based on the fitness values in 2.
4. If requirements are met, then stop. Otherwise go back to 2.

All these heuristic search methods, and their combinations, can significantly differ in total

number of sampling points that are needed to converge to the global minimum. In this work we will consider only the PSO algorithm and we give the rationale of why this method can perform better than a GA.

GAs build on the Darwinian concept of survival of the fittest, whereas the PSO philosophy is based on the concept of social influence and social learning. In a GA, a population of potential solutions selected at random samples the search space. The fittest solutions, i.e., those that show small values of the objective function, are selected for generation through crossover and (random) mutation, whereas the less-fit individuals are eliminated from the genetic pool. GA operators, such as random mutation and crossover, generate a new population of individuals whose positions are somewhat unpredictable and this can be a disadvantage when this position represents the location of a field measurement.

PSO algorithms, on the other hand, have been inspired by the observation of flocks of birds, swarms of insects, schools of fish, and other collective social behaviors. A swarm of particles is assigned a random position and velocity to sample the search space. The particle direction at the next "time" step is specified by a combination of the current particle direction, by the particle local minimum position, and by the swarm's global minimum position. Unlike in GAs, particles in PSO keep their individuality and can be tracked across time steps, allowing a more efficient allocation of the path traveled by technicians in the field when going from one point measurement to the next. Note that we have a steady-state seepage pattern but use a dynamic search strategy.

In Figure 7 we illustrate the application of the PSO algorithm (Birge, 2003) to the problem of finding the minimum of the correlation map generated by the ANN described in the previous

section. The objective function to be minimized is the regression coefficient between ANN model and field measurements for the CO_2 concentration. The search landscape is relatively flat because of the excellent ANN non-linear model of integrated background, except at the seepage anomaly, which can be seen at the coordinates (1000 m, 800 m) plotted in red where the CO_2 concentration (and flux) is anomalously high.

As shown in Figure 7, we used PSO to locate the CO_2 seepage anomaly in the virtual landscape. The position and velocity of four particles was initialized at random, and then the particles explored the search space according to the PSO rules as shown in the snapshots of the convergence process at different evolution steps in Figure 7. Current particle positions are plotted as white dots, while the global minimum is indicated by a red cross. Convergence to the global minimum was achieved in the majority of the runs for different random initializations. Additional analyses on the dependence of convergence on number of points, so-called velocity of particles, initial positions, etc. will need to be undertaken to understand better convergence and convergence rates. We stress that other minimization algorithms would fail in pinpointing this particular seepage anomaly because of the flat and noisy background with $L_s \sim L_i$.

6. Conclusions

1. Summary

Leakage of CO_2 from a geological storage site and its ultimate seepage into the atmosphere is a matter of concern for the effectiveness and public acceptance of CCS. In this work, we discussed strategies for field measurements that optimally characterize seepage, which may include determining that seepage is occurring and subsequently pinpointing its location and quantifying the seepage rate.

There are four characteristic length scales relevant to seepage characterization that, together with a prescribed maximum allowable seepage flux, amplification factor, and measured background respiration flux, can be used to estimate roughly the number of EC towers needed in a static grid for a given injection rate. Monitoring networks can be classified into two main classes, namely static and dynamic. The archetype of a static network is the grid (e.g., a grid of eddy covariance towers), whereas new measurement locations in a dynamic network depend on the history of the measurements. The static EC grid can be used to detect and roughly locate possible CO_2 seepage, although numerous EC towers may be required depending on the area of potential seepage, detection requirements, and background respiration. Pinpointing the locations of seepage can be done using a dynamic approach once seepage is detected and roughly located.

We used numerical simulations of a virtual site as an example case on which to apply pinpointing strategies. The seepage detection problem can be conveniently treated by means of Artificial Neural Networks (ANNs) that obviate the need for mechanistic understanding of the complex natural processes occurring to produce given background natural CO_2 fluxes and concentrations. ANNs provide a means to identify complex non-linear correlations between background CO_2 fluxes and concentrations, and other explanatory variables of hydrogeological, atmospheric, geophysical, and topographic type. We then defined seepage as an anomaly with respect to an expected background, and showed how seepage measurements are generally anti-correlated with expectations derived from the ANN model. This method provides a reliable way to identify seepage provided you know where to look.

The ANN method does not, however, provide a way to identify the next point to be measured in a dynamic network campaign with the objective of pinpointing seepage locations. For this, we propose application of a Particle Swarm Optimization (PSO) algorithm aimed at overcoming the

problem associated with the typically flat, multi-minima, and highly-localized global minima surfaces which are characteristic of natural ecosystem background fluxes and concentrations that will be encountered in CCS applications. PSO provides an efficient method to minimize the number of measurements and the total distance that the field technician needs to travel when going from one measurement point to the next.

2. Recommendations

Based on the results of this work, we recommend that monitoring networks be deployed in three distinct phases. The flow of the process is shown in Figure 8. Following definition of the monitoring objective, the first phase involves the deployment of a static monitoring network of, for instance, EC towers equally spaced according to the estimates obtained as a function of the admissible seepage rates and background respiration. The second phase, which can proceed in parallel with the first, involves the acquisition of finer-scale integrated background measurements, typically point measurements, which synthesize CO_2 flux or concentrations as a function of ecosystem explanatory variables in an ANN regressive model. If the static network detects a possible seepage signal, a third phase would be needed. In the third phase, deployment of a dynamic monitoring network would be aimed at pinpointing the precise location of the seepage through directed measurements, and quantifying it as to its magnitude and evolution.

While the findings and recommendations in this work were based solely on theory and modeling, the motivation for the work arises from the real-world application of CCS deployment to reduce CO_2 emissions to the atmosphere. Given the urgency needed to reduce CO_2 emissions, and the need to deploy CCS at minimal cost, research aimed at improving monitoring and measuring precision, along with advanced data analysis approaches as proposed in this study, will both help to lower the needed amplification factor and thereby increase the measurement length scales

needed. We recommend that novel methodologies be tested in ongoing field tests of CCS technologies as well as at natural analog sites. Improved methodologies based on field trials will be invaluable for developing cost-effective monitoring approaches.

Acknowledgments

We thank William J. Riley (LBNL) for assistance with the ISOLSM model computations and Jennifer L. Lewicki (LBNL) for constructive review comments. This work was carried out within the ZERT project, funded by the Assistant Secretary for Fossil Energy, Office of Sequestration, Hydrogen, and Clean Coal Fuels, National Energy Technology Laboratory, of the U.S. Department of Energy under Contract No. DE-AC02-05CH11231

References

Anderson, D., Farrar, C., Eddy covariance measurement of CO_2 flux to the atmosphere from an area of high volcanogenic emissions, Mammoth Mountain, California, *Chem. Geology*,177, 31–42, 2001.

Baldocchi, D., Wilson, K., Modeling CO_2 and water vapor exchange of a temperate broadleaved forest across hourly to decadal time scales, *Ecological Modelling*, 142, 155–184, 2001.

Benson, S.M., Myer, L.R., Monitoring to ensure safe and effective geologic sequestration of carbon dioxide, in *Intergov. Panel Clim. Change 2002. Workshop carbon capture storage. Proc. Intergov. Panel Clim. Change. Regina, Can. Petten, Neth.: Energy Res. Cent. Neth.*, 2002.

Benson, S.M., Monitoring carbon dioxide sequestration in deep geological formations for inventory verification and carbon credits, Society of Petroleum Engineers, *SPE-102833*, 2006 Annual Technical Conference and Exhibition, San Antonio TX, 24-27 September, 2006.

Birge, B., PSOt - a particle swarm optimization toolbox for use with Matlab, in *Swarm Intelligence Symposium, 2003. SIS '03. Proceedings of the 2003 IEEE*, pp. 182–186, 2003.

Chiodini, G., Cioni, G.R., Guidi, M., Raco, B., Marini, L., Soil CO_2 flux measurements in volcanic and geothermal areas, *Appl. Geochem.*, 13, 543–552, 1998.

Dorigo, M., Stützle, T., *Ant Colony Optimization*, Cambridge, MA: MIT Press/Bradford Books, 2004.

Eberhart, R. C., Kennedy, J., New optimizer using particle swarm theory, in *Proceedings of the Sixth International Symposium on Micromachine and Human Science, Nagoya, Japan*, pp. 39–43, 1995.

Ehman, J.L., Schmid, H.P., Grimmond, C.S.B., Randolph, J.C., Hanson, P.J., Wayson, C.A., and Cropley, F.D.. An initial intercomparison of micrometeorological and ecological inventory estimates of carbon exchange in a mid-latitude deciduous forest, *Global Change Biology*, *(6)*, 575—589, 2002, doi:10.1046/j.1365-2486.2002.00492.x.

Foken, T., Wichura, B., Tools for quality assessment of surface-based flux measurements, *Agric. For. Meteorol.*, 78, 83–105, 1996.

Gouldin, M., Crill, P., Automated measurements of CO_2 exchange at the moss surface of a black spruce forest, *Tree Physiology*, 17, 537–542, 1997.

Govindaraju, R., Rao, A., *Artificial Neural Networks in Hydrology*, Springer, 2000, iSBN-10: 0792362268.

Hagen, S.C., Braswell, B.H., Linder, E., Frolking, S., Richardson, A.D., Hollinger, D.Y., Statistical uncertainty of eddy flux-based estimates of gross ecosystem carbon exchange at Howland Forest, Maine,, *J Geophys Res-Atmos*, , D08S03, doi:10.1029/2005JD006,154, 2006.

Hansen, J., Defusing the global warming time bomb, *Scientific American*, *(3)*, 00368,733, 2004.

Hepple, R.P., Benson, S.M., Geologic storage of carbon dioxide as a climate change mitigation strategy: performance requirements and the implications of surface seepage, *Environ. Geol.*, , 576—585, 2005, DOI 10.1007/s00254-004-1181-2.

Holland, J., *Adaptation in Natural and Artificial Systems*, MIT Press, 1992, iSBN-10:0-262-58111-6.

Intergovernmental Program on Climate Change (IPCC) Special Report on carbon dioxide capture and storage, ISBN 92-969-119-4, http://www.ipcc.ch/activity/srccs/index.htm, 2005.

Lewicki, J., Hilley, G., Oldenburg, C.M., An improved strategy to detect CO_2 leakage for verification of geologic carbon sequestration, *Geophys. Res. Lett.*, *(19)*, Art. No. L19,403, 2005.

Markou, M., Singh, S., Novelty detection: a review - part 1: statistical approaches, *Signal Processing*, *12*, 2481–2521, 2003a.

Markou, M., Singh, S., Novelty detection: a review - part 2: neural network based approaches, *Signal Processing*, *12*, 2499–2521, 2003b.

Massmann, W., Lee, X., Eddy covariance flux corrections and uncertainties in long term studies of carbon and energy exchanges, *Agric. For. Meteorol.*, 113, 121–144, 2002.

Miles, N.M., Davis, K.J., Wyingaard, J.C., *Detecting leaks from belowground CO_2 reservoirs using eddy covariance*, chap. 21, pp. 1031–1044, Elsevier, Ltd., 2005.

Myer, L.R., Hoversten, G.M., Gasperikova, E., Sensitivity and cost of monitoring geologic sequestration using geophysics, Proc. *Sixth Annual International Conf. on Greenhouse Gas Control Technologies*, Gale, J., and Kaya, Y. (eds.), 1-4 October 2002, Pergammon, 1, 377-382.

Oldenburg, C.M., A.J.A. Unger, On leakage and seepage from geologic carbon sequestration sites: unsaturated zone attenuation, *Vadose Zone Journal*, 2(3): 287-296, August 2003.

Oldenburg, C.M., J.L. Lewicki, R.P. Hepple, Near-surface monitoring strategies for geologic carbon dioxide storage verification, Lawrence Berkeley National Laboratory Report *LBNL-54089,* October 2003.

Oldenburg, C.M., A.J.A. Unger, Coupled vadose zone and atmospheric surface-layer transport of CO_2 from geologic carbon sequestration sites, *Vadose Zone Journal*, *3*, 848–857, 2004.

Pacala, S., Socolow, R., Stabilization wedges: Solving the climate problem for the next 50 years with current technologies, *Science (5686)*, 968–972, 2004.

Pruess, K., Oldenburg, C.M., Moridis, G.J.. TOUGH2 User's Guide Version 2. E. O. Lawrence Berkeley National Laboratory Report *LBNL-43134*, November 1999.

Radziemski, L., Solarz, R., Paisner, J., *Laser Spectroscopy and Its Applications*, no. 11 in Optical Engineering Series, Marcel Dekker, NY, 1987.

Riley, W.J., Still, C.J., Torn, M.S., Berry, J.A., A mechanistic model of $H_2{}^{18}O$ and $C^{18}OO$ fluxes between ecosystems and the atmosphere: Model description and sensitivity analyses. *Global Biogeochemical Cycles*. 16, Art. No. 1095, doi 10.1029/2002GB001878, 2002.

Riley, W.J., Still, C.J., Helliker, B.R., Ribas-Carbo, M., Berry, J.A. ^{18}O composition of CO_2 and H_2O ecosystem pools and fluxes in a tallgrass prairie: Simulations and comparisons to measurements, *Global Change Biology*. 11. 1567–1581, 2003.

Schlessinger, M., *Infrared Technology Fundamentals*, no. 46 in Optical Engineering Series, Marcel Dekker, Inc., New York, NY, 1995.

Shackley, S., Waterman, H., Godfroij, P., Reiner, D., Anderson, J., Draxlbauer, K., Flach, T., *Energy Policy*, in press, 2007.

Shuler, P., Tang, Y., Atmospheric CO_2 monitoring systems, in *Carbon Dioxide Capture for Storage in Deep Geologic Formations*, Vol. 2, D.C. Thomas and S.M. Benson, eds., pp 1115–1130, Elsevier, 2005.

Storn, R., Price, K., Differential evolution - a simple and efficient adaptive scheme for global optimization over continuous spaces, *Technical Report TR-95-012*, ICSI, 1995.

Figure Captions

Figure 1. The schematic illustrates different length scales involved in the monitoring process. L_x is a measure of the maximum extent of the monitoring area; L_m are measures of monitoring footprints; L_i are measures of the area of influence around the seepage area; and L_s is the scale of the main seepage area.

Figure 2. Model of net CO_2 fluxes showing hourly variation for conditions similar to the ones of the Morgan Monroe State Forest, Indiana (USA). Average night-time values are shown in red.

Figure 3. False-color satellite photo of the virtual injection site. The image has been altered to extract vegetation levels by analyzing the green hues.

Figure 4. TOUGH2 simulations for the virtual site. (a) Elevation map of the virtual site; (b) Soil-water saturations at 10 cm depth; (c) CO_2 concentration levels at 10 cm depth derived from the fluxes imposed at the water-table level; (d) Super-position of the CO_2 concentration in (c) and elaboration of the vegetation signal depicted in Figure 3.

Figure 5. Saturation vs. elevation for the numerical simulations (dots). The blue and red lines represent a two- and three- node ANN regression, respectively. The regression coefficients were equal to 0.992 *and* 0.999 *, respectively.*

Figure 6. Application of the ANN technique. Left: The array of red dots represents a set of CO_2 concentration measurements in undisturbed conditions. Measurements at the purple dots are taken as a validation set for the ANN model. The green dots represent measurements taken along a line crossing the anomalous seepage footprint. Right: Results of the ANN regression model. The explanatory variables are the saturation field in Figure 4 and the vegetation map in Figure 3. The ANN provides an excellent model for the undisturbed measurements (red dots) and for the validation set (purple dots). The measurements across the anomalous seepage footprint (green dots) are anti-correlated with the ANN model and clearly indicate the presence of an anomaly.

Figure 7. Application of the PSO algorithm to the optimal detection of a seepage anomaly. Four particles (white dots) are initiated at random (top left) to explore the search space according to the PSO rules. The evolution of the panels is from left to right and from top to bottom. The global minimum of the particle swarm (red cross) converges consistently towards the function minimum indicated by the red seepage anomaly.

Figure 8. Flow of field monitoring and measuring showing the steps of detection, pinpointing, and quantification.

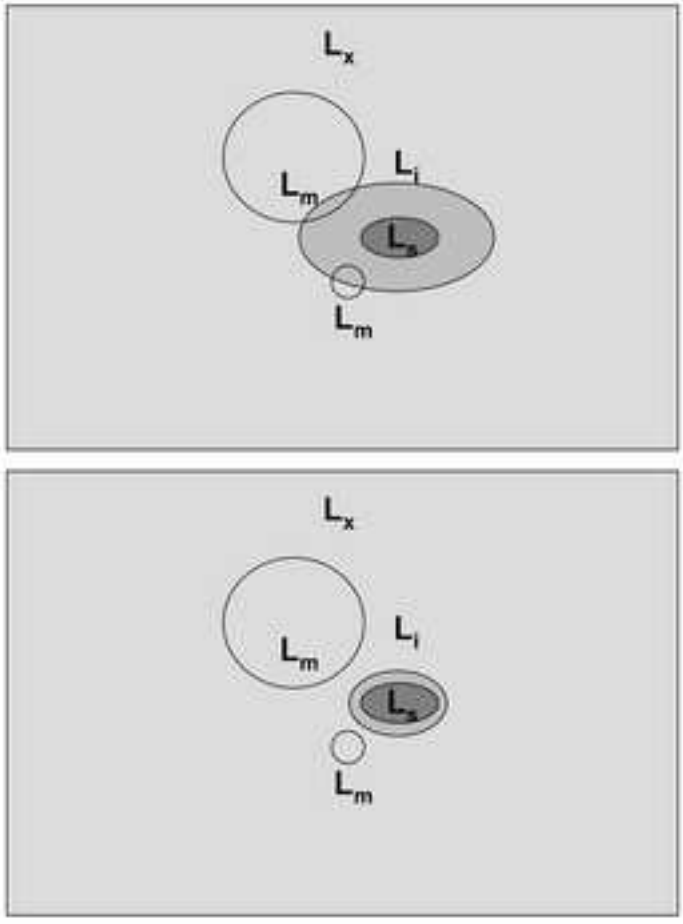

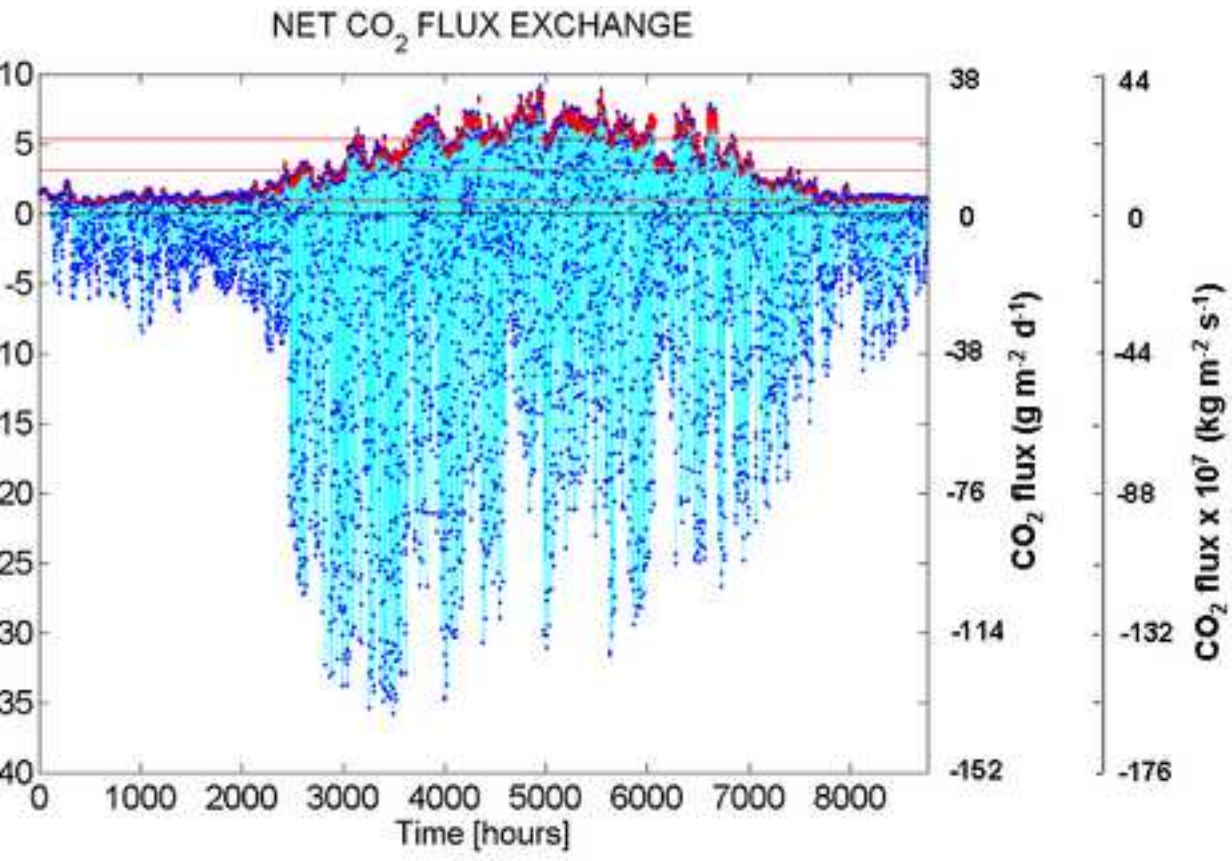

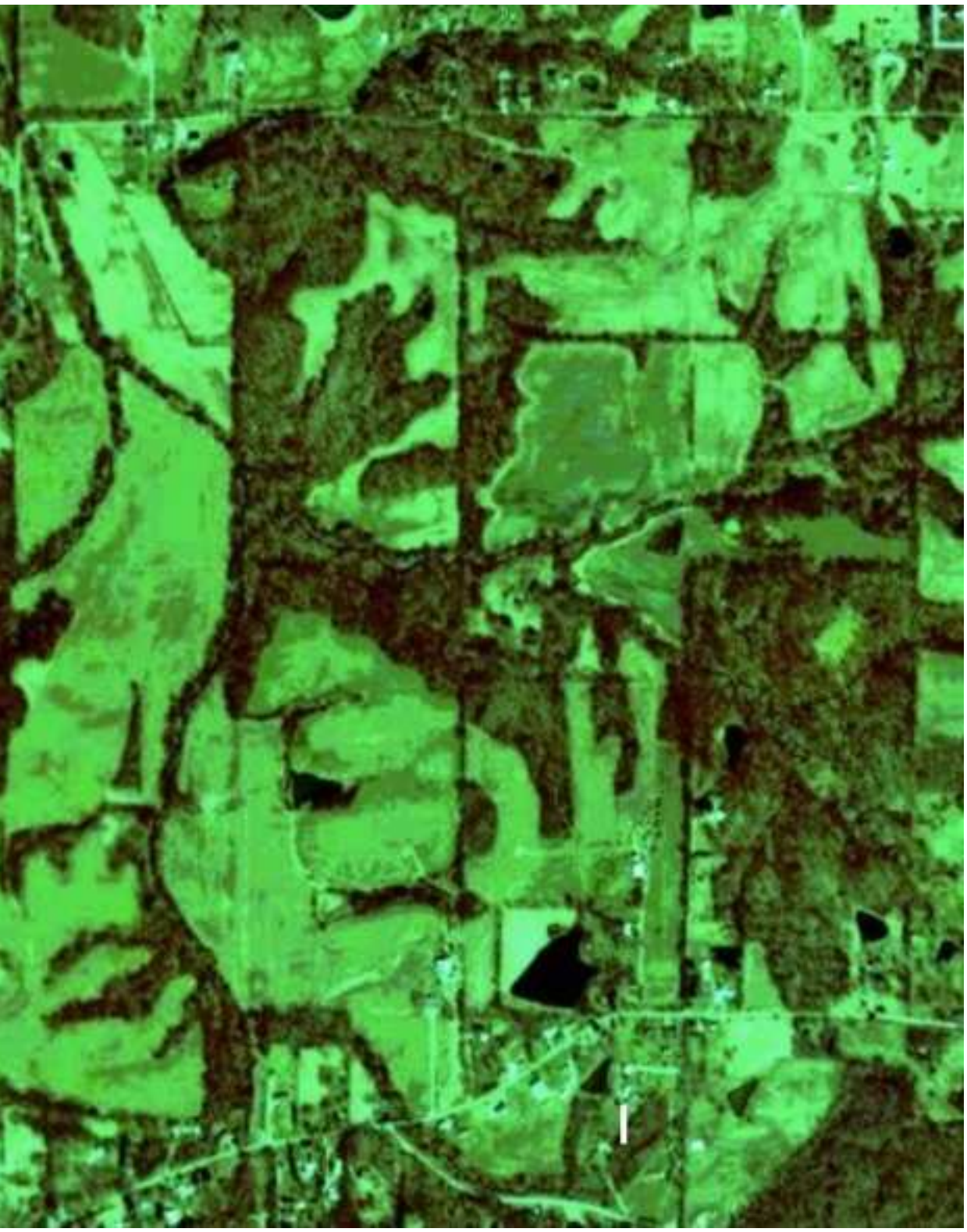

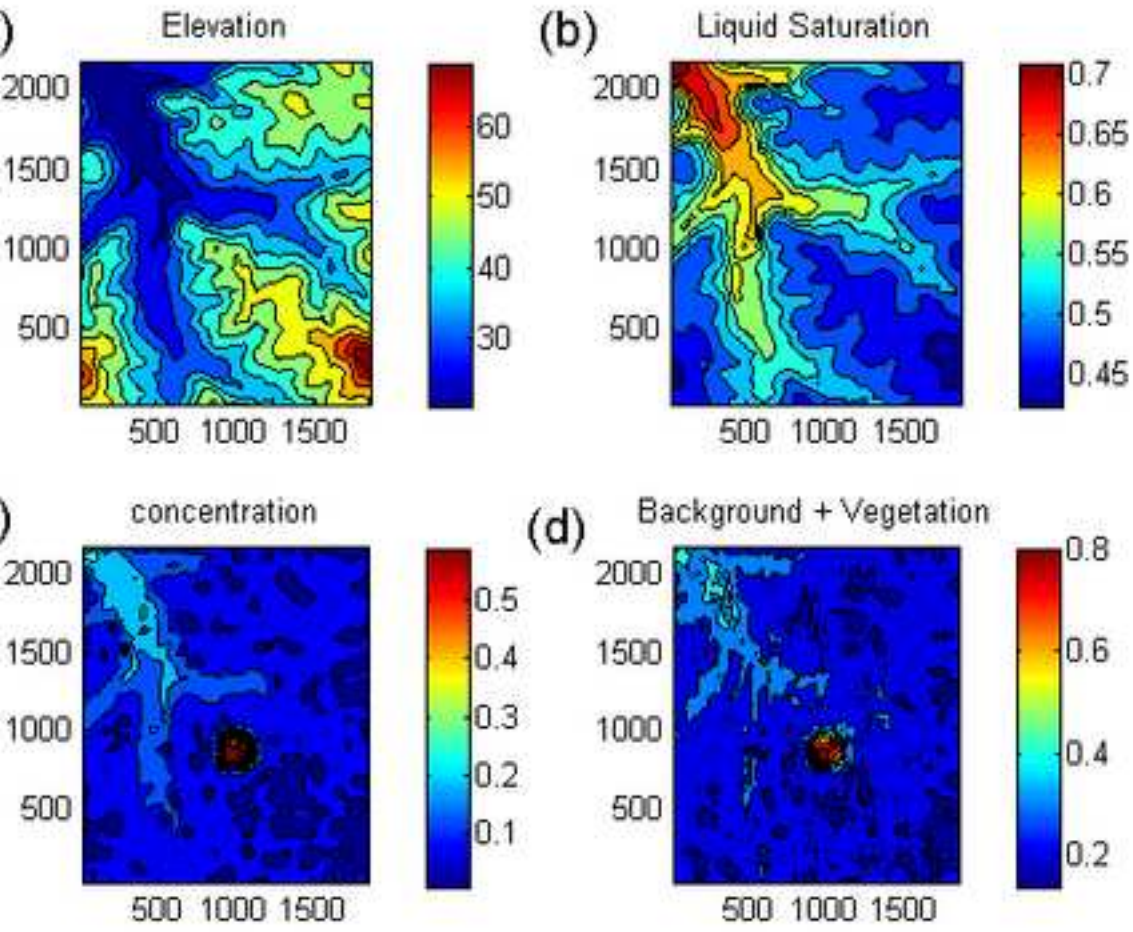

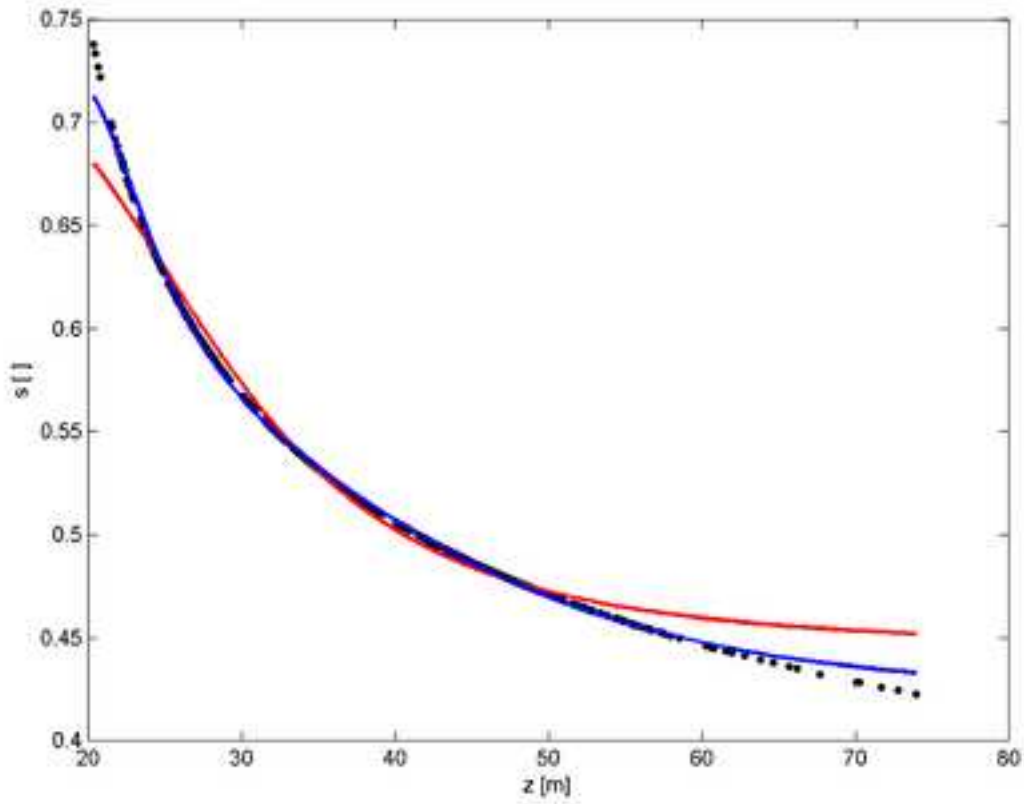

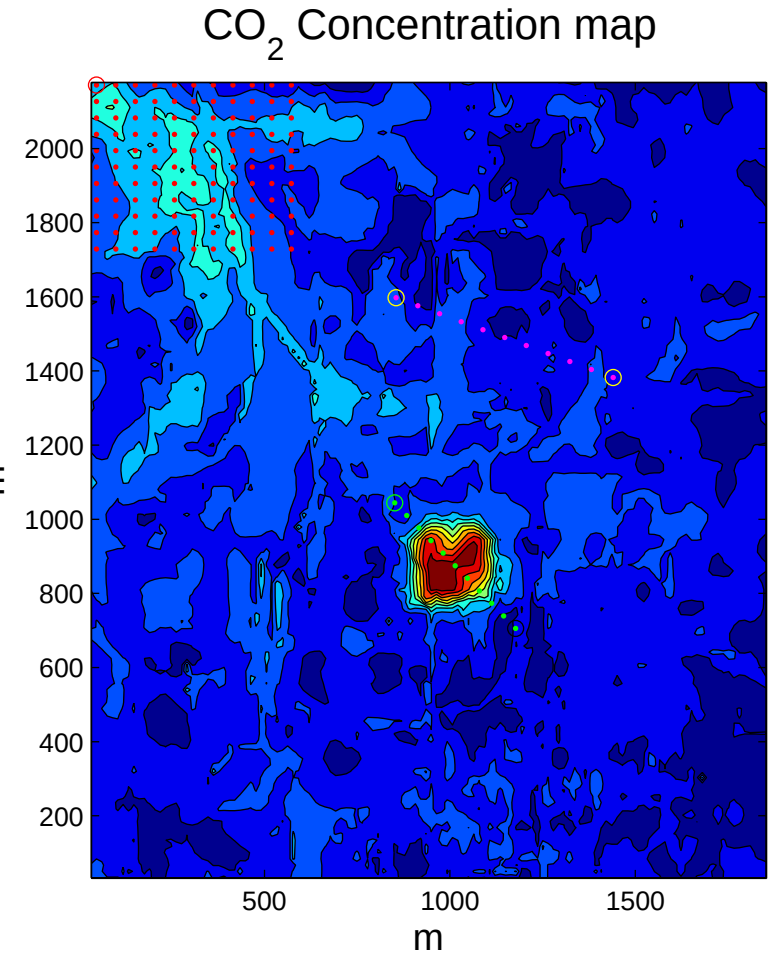
CO_2 Concentration map
2000
1800
1600
1400
1200
1000
800
600
400
200
500
1000
1500
m

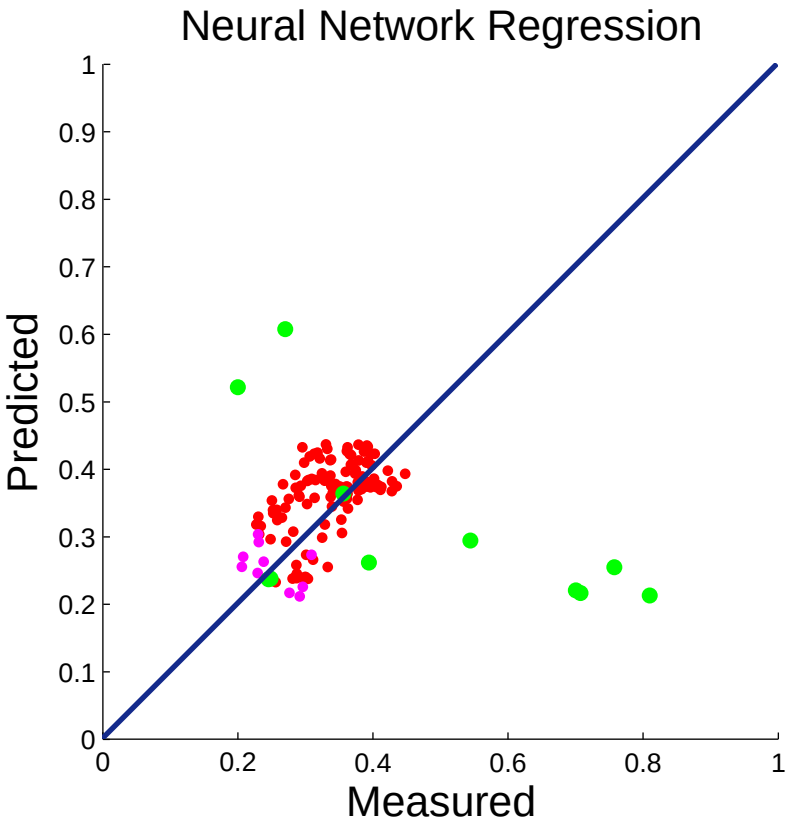
Neural Network Regression
Predicted
Measured
0
0.1
0.2
0.3
0.4
0.5
0.6
0.7
0.8
0.9
1
0.2
0.4
0.6
0.8

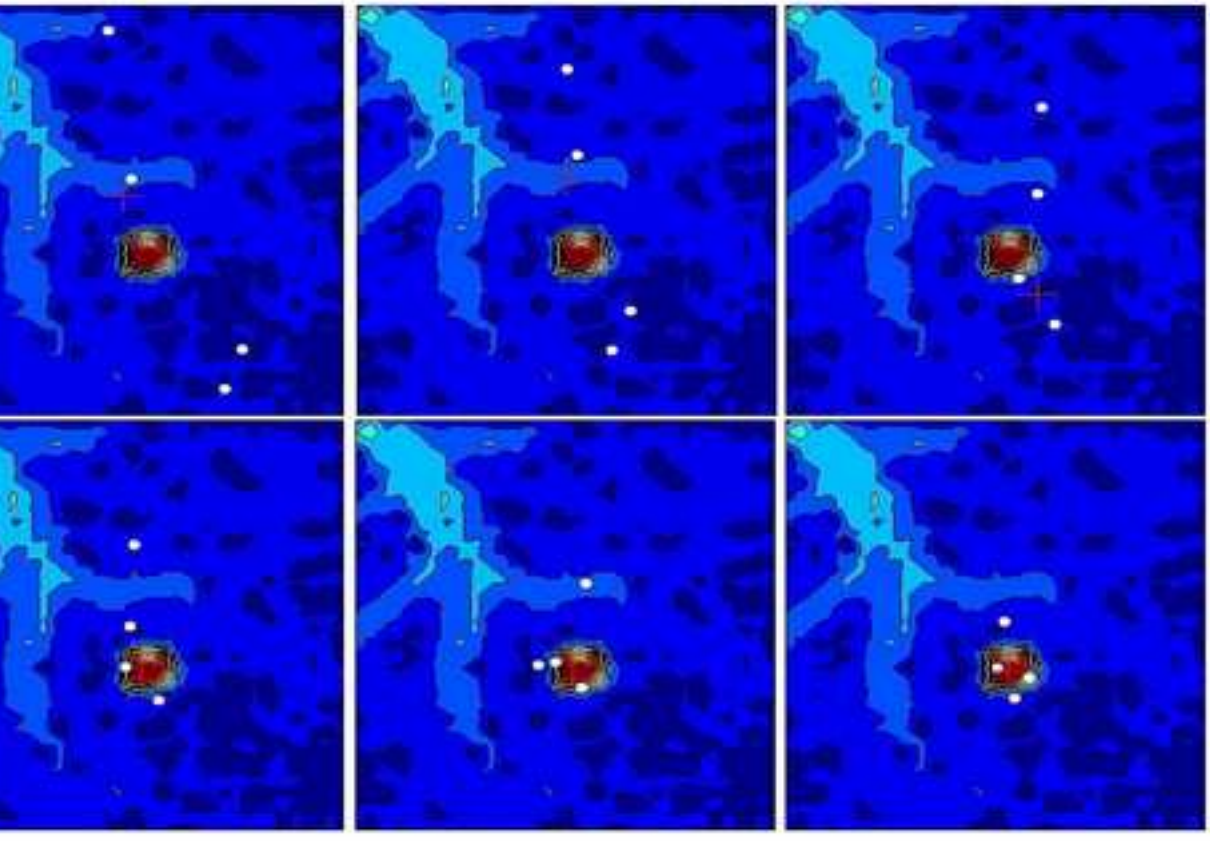

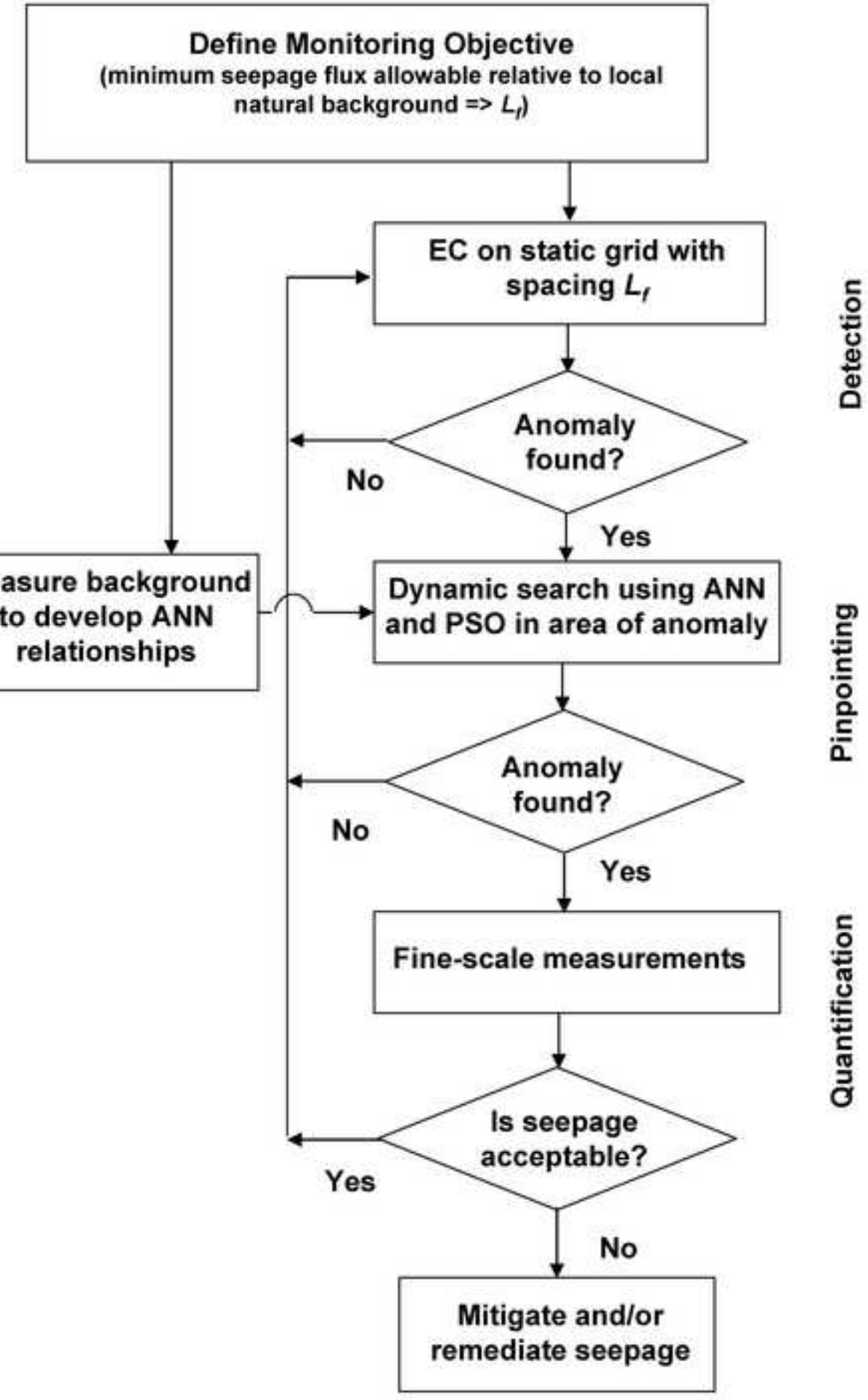

Table 1. L_m (m) after 25 years and n_{tower} (in parentheses) for j_r = 5 μmol m^{-2} s^{-1} as a function of λ and release fraction R from CO_2 storage for a 1 GW coal-fired power plant.

	$\lambda=2$	$\lambda=5$	$\lambda=10$
$R=10^{-2}$	*19000* **(1)**	*9500* **(2)**	*6327* **(3)**
$R=10^{-3}$	*6000* **(4)**	*3000* **(13)**	*2000* **(29)**
$R=10^{-4}$	*1900* **(32)**	*950* **(127)**	*632* **(284)**

Table 2. L_m (m) after 25 years and n_{tower} (in parentheses) for j_r = 20 μmol m^{-2} s^{-1} as a function of λ and release fraction R from CO_2 storage for a 1 GW coal-fired power plant.

	$\lambda=2$	$\lambda=5$	$\lambda=10$
$R=10^{-2}$	*9500* **(2)**	*4700* **(6)**	*3160* **(12)**
$R=10^{-3}$	*3000* **(13)**	*1500* **(51)**	*1000* **(114)**
$R=10^{-4}$	*950* **(127)**	*475* **(505)**	*316* **(1136)**